Neural, Parallel, and Scientific Computations 22 (2014) 303-314

INTERACTION OF WIND WITH SURFACE WATER WAVES

F. DRULLION[1] AND S. G. SAJJADI[1,2]

[1]Department of Mathematics, Embry Riddle Aeronautical University, USA.
[2]Trinity College, University of Cambridge, UK.
Corresponding author: Frederique Drullion (drulliof@erau.edu)

ABSTRACT. A turbulent flow over different growing and non growing water waves is considered by constructing a high-Reynolds-number stress closure model. The profile of the water wave as well as the associated orbital velocities are prescribed. In the case of a growing wave, the profile and the orbital velocities can change dynamically under the action of the wind blowing above the wave. This work focuses on the influence of the wave age (ratio of the wave speed over the wall friction velocity) and the wave steepness on the dynamics of the critical layer (the region about the height at which the real part of the complex wave phase speed is equal to the mean flow velocity) and on region of close streamlines, called cat's eye patterns that are created above the surface of the wave and is centered about the critical layer. The simulations show that the height of the critical layer increases with the wave age and the steepness of the wave, what is in agreement with the direct numerical simulations reported by Sullivan *et al.*[21]. The cat's eye patterns increase in size and extend vertically with the increase of the wave age and lead to a maximum disturbance of the mean flow for older waves. The model being computationally less expensive than a DNS approach, it allowed us to study waves growing under the influence of the wind. The simulations show that as the wave grows the critical layer elevates and the cat's eye structures become larger leading again to an important disturbance of the wind flow above the wave.

AMS (MOS) Subject Classification. 76D10, 76D33, 76M12.

1. Introduction

The process of wind generated waves growth and decay has been a subject of many studies for decades but despite theoretical studies, experiments and numerical simulations the question of the energy transfer between the wind and the water waves remains very controversial. In 1957 Miles was the first to give a quantitative description for the growth of wind generated waves [16]. But in his theory the interaction between wave-induced motions in the air flow and the turbulence is neglected, turbulence serves only to maintain a logarithmic wind profile. A specific region called the critical layer is at the center of Miles theory and of Lighthill interpretation of wave growth [11]. The critical layer is the region about the critical height ζ_c defined as the height at which the real part of the complex wave phase speed c $(= c_r + ic_i)$ is equal

Received July 9, 2014

to the mean flow velocity. Mile states that the energy is transferred from the wind to a wave at a rate that is proportional to the curvature of the velocity profile at the critical height. The main focus of this work is to study the dynamic of the critical layer above different water waves.

Numerical simulations of a flow over waves based on the Reynolds Averaged Navier-Stokes equations were carried out by Gent and Taylor [7] who used a one equation turbulence model and Al-Zanadi & Hui [1] who used a two-equation eddy viscosity closure for turbulence. In the 90's, Mastenbroek *et al.* [15] applied a second-moment Reynolds stress turbulence closure for the turbulent flow over water waves and compared it to a k–ε model. They show that wave growth is very sensitive to the turbulence model used. Belcher and Hunt compiled a review of the different turbulence model used for turbulent flow over hills and waves [2]. In the 90's, some direct numerical simulations have been carried out to study the turbulent flow over stationary wavy surfaces [13],[4],[3]. As the wavy surface was stationary these simulations could not be applied to ocean water waves. More recently direct numerical simulations of flows over idealized water waves have been performed, eliminating the sensitivity to the turbulence closure model [5],[12]. In 2000 Sullivan *et al.* [21], developed a three-dimensional DNS model to study turbulent flows over idealized water waves. They studied the influence of the wave on the mean flow depending on the wave age $c/U*$ (wave speed over the wall friction velocity) and the wave slope ak. They pointed out the importance of the region of closed streamlines also called cat's eye pattern centered at the critical layer height. For young waves (small c/U_*) the cat's eye pattern is centered upwind of the trough and extend almost all the way to the surface of the wave. As the wave age increases the cat's eye centers move upstream, the pattern expands in the vertical direction and the structures are formed well above the water surface causing a maximum of disturbance to the mean streamlines.

Direct numerical simulations have the irrefutable advantage of not depending on the turbulence closure model but the very high computational cost associated with them only allows, for now, to study non growing idealized monochromatic wave profiles. In order to get a little closer to reality and following the study of Sajjadi *et al.* [20], we present here, a computational study of turbulent flow over growing water waves with varying slopes ka and different wave ages c_r/U_*, using a differential second-moment turbulence closure model. The initial shape of the water surface is prescribed but the wave profile as well as the orbital velocities can evolve dynamically under the action of the air flow above the surface.

After presentation of the governing equations and of the numerical model, our results for a moving non growing monochromatic wave are presented and compared to the ones obtained by Sullivan with his DNS simulations [21]. We will look at the

influence of the wave age and wave slope on the dynamic of the critical layer. After validation of the model we will investigate monochromatic moving and growing waves.

2. **Problem formulation**

We consider a deep water surface wave moving at the speed $c_r = \sqrt{\frac{g}{k}}$ and a wind with a logarithmic profile blowing above the wave. At the height of one wavelength above the surface of the wave, the wind velocity is imposed to be U_λ .

The turbulent flow has a mean velocity profile $U(\zeta) = U_1 \ln(\zeta/\zeta_0)$ where $U_1 \equiv U_*/\kappa$, U_* is the friction velocity , κ is von Kármán's constant and ξ and ζ are the wave-following coordinate through the transformation

$$x = \xi, \qquad z = \zeta + h(\xi, \eta), \tag{2.1}$$

where $h = h(\xi, \eta)$ maps $z = h_0$ on $z\eta = 0$ and is evanescent for $k\zeta \uparrow \infty$ but is otherwise arbitrary. The wave is assumed to be periodic in the x-direction, it has a wavelength λ, an amplitude a and a slope $ak = 2\pi/\lambda$. In our simulations, the frame of reference is traveling with the wave. The wave is monochromatic with an initial surface profile given by $h(\mathscr{X}, t) = a(t) - a(t)\cos[k\mathscr{X}]$, where $\mathscr{X} = \xi - c_r t$

3. **Equations of motion**

The flow of air with density ρ_a and kinematic viscosity ν_a over water waves is governed by the Reynolds averaged Navier-Stokes equations, which for an incompressible fluid may be expressed in the Cartesian form as

$$\frac{\partial U_i}{\partial x_i} = 0 \tag{3.1}$$

$$\frac{DU_i}{Dt} = -\frac{1}{\rho_a}\frac{\partial P}{\partial x_i} + \frac{\partial}{\partial x_j}\left[\nu_a\left(\frac{\partial U_i}{\partial x_j} + \frac{\partial U_j}{\partial x_i}\right) - \overline{u_i' u_j'}\right] \tag{3.2}$$

where U_i is the mean velocity component in the x_i-direction, P is the mean pressure, $\overline{u_i' u_j'}$ is the Reynolds-averaged stress correlation and t is time.

The air is assumed to be flowing over an unsteady surface wave, propagating along the positive ξ-axis and whose elevation h is given by

$$h(\xi, t) = a(t)\cos[k(\xi - ct)]$$

c is the complex phase speed.

In order to close equation (3.2), a model for the Reynolds-averaged stress correlations must be provided *a priori*. A rational approach for providing a model for

$\overline{u_i'u_j'}$ in equation (3.2) relies on its *exact* transport equation, which may be cast in the following form

$$\frac{D\overline{u_i'u_j'}}{Dt} = P_{ij} + \Pi_{ij} - \varepsilon_{ij} + d_{ij} \tag{3.3}$$

where $P_{ij} = -(\overline{u_i'u_k'}\partial U_j/\partial x_k + \overline{u_j'u_k'}\partial U_i/\partial x_k)$ is the production term, Π_{ij} represents the velocity-pressure gradient correlation, ε_{ij} the viscous dissipation, and d_{ij} represents diffusion by both molecular viscosity and the triple velocity moments.

On the left-hand side of (3.3), the stress convection, and the production term are both exact and require no further modelling. However, all other terms contain further unknowns which must be modelled. For this we adopt a high-Reynolds-number turbulence model [18].

In this model, the pressure correlation Π_{ij} is decomposed into a redistributive part, ϕ_{ij}^*, and a non-redistributive part by

$$\Pi_{ij} \equiv -\frac{1}{\rho_a}\left(\overline{u_i'\frac{\partial p'}{\partial x_j} + u_j'\frac{\partial p'}{\partial x_i}}\right) = \phi_{ij}^* + \frac{\overline{u_i'u_j'}}{2K}d_{kk}^p \tag{3.4}$$

where $d_{kk}^p = -(1/\rho_a)\partial\overline{u_k'p'}/\partial x_k$ represents the pressure diffusion of the turbulent kinetic energy $K = \frac{1}{2}\overline{u_i'u_i'}$.

The model employed for the redistributive part of the pressure correlation, ϕ_{ij}^*, is based on the cubic realizable form derived by Fu [6].

The dissipation ε_{ij} is modelled as

$$\varepsilon_{ij} = \left(1 - A^{1/2}\right)\frac{\varepsilon}{K}\overline{u_i'u_j'} + {}^2\!/_3\varepsilon\delta_{ij} \tag{3.5}$$

where $A = 1 - 9/8(A_2 - A_3)$, $A_2 = a_{ij}a_{ij}$, $A_3 = a_{ij}a_{jk}a_{ki}$ and $a_{ij} = \overline{u_i'u_j'}/K - {}^2\!/_3\delta_{ij}$

This is very similar to the form adopted in other high-Reynolds-number flows, see for example Gibson & Launder [8].

In (3.5) The dissipation rate ε is obtained from the solution of its own transport equation:

$$\begin{aligned}\frac{D\varepsilon}{Dt} &= c_{\varepsilon 1}\frac{\varepsilon P_{kk}}{2K} - c_{\varepsilon 2}\frac{\varepsilon^2}{K} + \frac{\partial}{\partial x_l}\left[\left(\nu_a\delta_{lk} + c_\varepsilon\overline{u_l'u_k'}\frac{K}{\varepsilon}\right)\frac{\partial\varepsilon}{\partial x_k}\right] \\ &\quad + c_{\varepsilon 3}A^{1/2}(1-A)\frac{\varepsilon}{\sqrt{K}}\overline{u_i'u_j'}\frac{\partial A}{\partial x_i}\frac{\partial}{\partial x_j}\left(\frac{K^{3/2}A^{1/2}}{\varepsilon}\right)\end{aligned} \tag{3.6}$$

with coefficients

$$c_{\varepsilon 1} = 1.0,\ \ c_{\varepsilon 2} = 1.92/(1 + 0.7A_dA_2^{1/2}),\ \ A_d = \max(0.2, A),\ \ c_{\varepsilon 3} = 1.0,\ \ c_\varepsilon = 0.18$$

The only remaining term in the stress transport equations is the diffusion term

$$d_{ij} = \frac{\partial}{\partial x_k}\left(\nu_a\frac{\partial\overline{u_i'u_j'}}{\partial x_k} - \overline{u_i'u_j'u_k'}\right) \tag{3.7}$$

The viscous diffusion is, of course, exact, and the triple correlations are modelled as proposed in Hanjalic & Launder [9]

$$\overline{u_i' u_j' u_k'} = -c_s \frac{K}{\varepsilon} \left[\overline{u_i' u_l'} \frac{\partial \overline{u_j' u_k'}}{\partial x_l} + \overline{u_j' u_l'} \frac{\partial \overline{u_i' u_k'}}{\partial x_l} + \overline{u_k' u_l'} \frac{\partial \overline{u_j' u_i'}}{\partial x_l} \right] \tag{3.8}$$

where $c_s = 0.11$.

4. **Numerical schemes**

The governing equations are solved using the finite volume method. The volumes are non-orthogonal and collocated such that all flow variables are stored at one and the same set of nodes. The numerical scheme uses a pressure based solver, approaching iteratively the solution using a semi-implicit method for pressure linked equations [17].

We have used a first order forward discretization in time, and the convective fluxes are approximated with the higher-order upstream-weighted scheme, QUICK of Leonard [10]. The pressure and diffusive fluxes are discretized using a central difference operator.

The finite volume method and the chosen discretizations lead to penta-diagonal equation in 2D, those systems are solved using a generalized version of tri-diagonal matrix algorithm (TDMA).

The discretization is proceeded by a transformation of the Cartesian coordinates of the governing equations to the non-orthogonal coordinates ξ and ζ using the Jacobian transformation matrix. The transport equation for any scalar property Φ many be expressed in non-orthogonal direction as

$$\underbrace{\frac{\partial}{\partial t}(J\rho_a\Phi)}_{\text{transient term}} + \underbrace{\frac{\partial}{\partial \xi}\left(\rho_a U^{(\xi,\zeta)}\Phi\right) + \frac{\partial}{\partial \zeta}\left(\rho_a W^{(\xi,\zeta)}\Phi\right)}_{\text{convection}} + \underbrace{\frac{\partial}{\partial \xi}\left(\alpha_\Phi J \frac{\partial \Phi}{\partial \xi}\right) + \frac{\partial}{\partial \zeta}\left(\beta_\Phi J \frac{\partial \Phi}{\partial \zeta}\right)}_{\text{diffusion}} = \underbrace{JS_\Phi}_{\text{source}} \tag{4.1}$$

where $U^{(\xi,\zeta)} = Uz_\zeta - Wx_\zeta$ and $W^{(\xi,\zeta)} = Wx_\xi - Uz_\xi$ are contravarient velocity components, J is the Jacobian of the transformation, S_Φ is the source term including diffusive terms, pressure terms in the momentum equation, $\alpha_\Phi = \Gamma_\Phi(x_\zeta^2 + z_\zeta^2)$, $\beta_\Phi = \Gamma_\Phi(x_\xi^2 + z_\xi^2)$, where Γ_Φ is isotropic diffusivity, and the subscripts ξ, ζ denote partial differentiations.

The mesh covering the computational domain contains 100×50 nodes and extends over six wavelengths in horizontal direction and one wavelength in the vertical direction. It is refined near the water surface in order to capture the steep gradients which are inherently present there. After a parameter analysis, this mesh size was chosen because it was the smaller size that ensured grid independent results.

5. **Boundary conditions**

At the top of the computational domain:

The mean velocities are

$$(U, W) = (U_\lambda - c_r, 0)$$

(due to the fact that the frame of reference is moving with the wave at the phase speed c_r). The vertical gradients of K, ε and normal stresses are set to zero. The turbulent shear stress is $\overline{u'w'} = 0$.

At the water surface the mean velocity components are matched (to first order in ka to orbital velocities:

$$U = -c_r ka \cos(k\mathscr{X}) - c_r, \qquad W = -c_r ka \sin(k\mathscr{X})$$

Note that when $c_r = 0$ the lower boundary conditions reduce to non-slip condition, which implies the wave is stationary. But as the wave is unsteady it can still grow as a result of shear flow above it if $c_i \neq 0$.

The air flow is assumed to be periodic in the horizontal direction, so periodic boundary conditions are imposed to all mean variables, turbulent stresses and the turbulent dissipation rate.

6. **Results**

6.1. **Non growing monochromatic waves.** In a first time, the wave shape and the orbital velocity are considered time independent. Figure (1) displays the streamlines obtained from the velocity field and shows the influence of the wave age on the critical layer. For these numerical simulations the waves steepness remains constant at $ak = 0.1$ and the "modified wave ages" c_r/u_λ (instead of the classic wave age c_r/U_*) varies between 0 and 0.47. For each wave age the height of the critical layer is represented by a white line. First, it can be seen that for a wave age of zero, that is for a stationary wave, at this steepness, there is no flow separation. There is also no cat's eye pattern and so no critical layer near the surface of the wave. For a moving wave ($c_r/U_\lambda > 0$), as the wave age increases the streamlines patterns change rapidly. At small wave age ($c_r/U_\lambda = 0.04$) the cats eyes structures appear and are then located very close to the surface. They are centered slightly upwind of the through. The critical layer is thinner in the windward side of the wave and thicker on the leeward side of the wave. As the wave age increases ($c_r/U_\lambda = 0.14$), the height of the critical layer increases. The cat's eye patterns elevate in the vertical direction. The critical layer is now less asymmetrical than at a lower wave age. As the wave age increases even more ($c_r/U_\lambda = 0.47$), the cat's eye structures extend all the way to the crest of

the wave; the structures grow in size (can get bigger than the wave amplitude) and extend even more in the vertical direction for a maximum disturbance of the mean flow. The wind flow does not follow at all the profile of the wave anymore. At this wave age the critical layer is almost flat and independence of the horizontal position. These observations are in agreement with the results obtained by Sullivan *et al.*

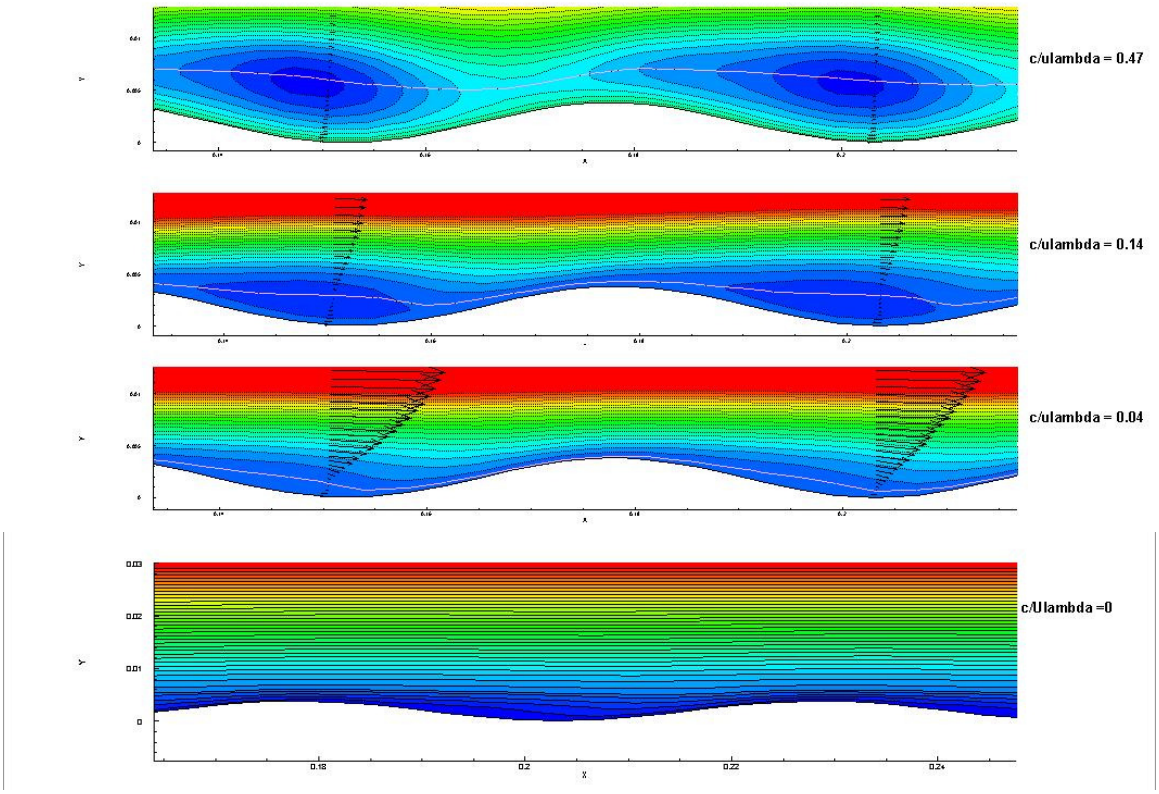

FIGURE 1. Streamlines pattern for different wave ages and constant steepness of 0.1

Figure (2) displays the pressure contours and shows how the surface wave affects the pressure field for a monochromatic wave with $ka = 0.1$ and $c_r/U_\lambda = 0.47$. The height of the critical layer is represented by a white line. At this steepness and this wave age, the critical layer has the greatest impact on the velocity field what is also in agreement with the DNS simulation results obtained by Sullivan *et al.*. At a wave age of 0.47 the pressure contours depict a marked hilting in the streamwise direction below the critical layer, above the critical layer the pressure contours bend back as the upstream direction, in accordance with Sullivan *et al.* observations. Figure (3) illustrates the influence of the steepness on the critical layer by showing the streamline patterns for a fixed wave age $c/U_\lambda = 0.47$ and for three different wave steepness, $ka = 0.1, 0.2$ and 0.3 (bottom to top). As the steepness increases, the height of the critical layer height increases and the cats eye structures extend vertically, as suggested by Sajjadi, Hunt & Drullion [20]. At low steepness, the structures extend horizontally over the crest while for a larger steepness the are more centered over the

through for a maximum disturbance o the mean flow.

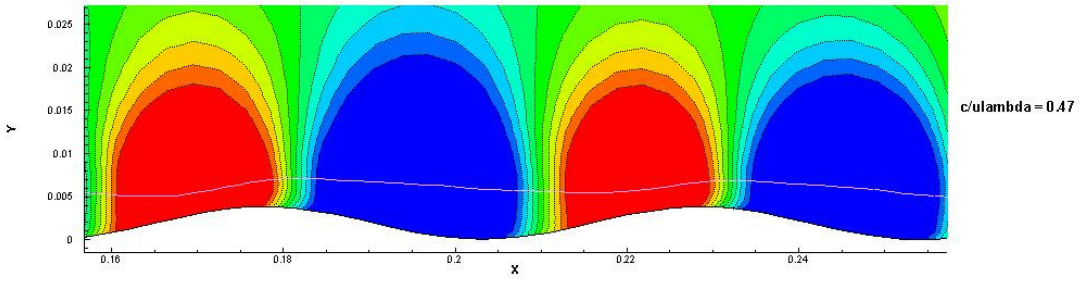

FIGURE 2. Pressure field at an alternate wave age of 0.47 and a teepness of 0.1

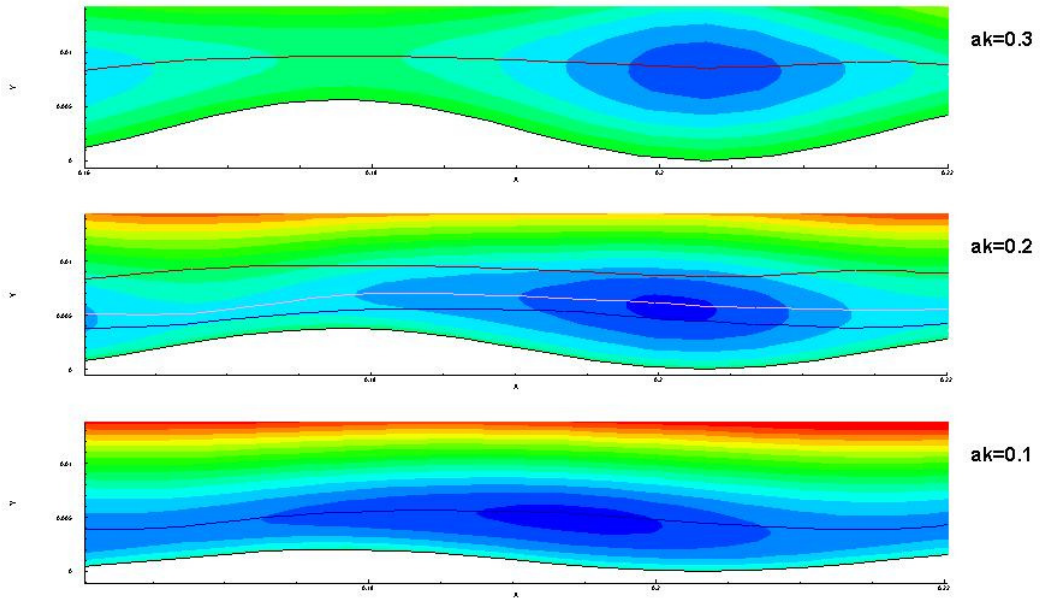

FIGURE 3. Streamlines for an alternate wave age of 0.47 and different steepnesses.

Ocean waves are not only moving but also growing and their steepness is changing as they travel. As the steepness of the wave is definitely having an effect on the critical layer, it is important to study waves changing in amplitude.

6.2. **Growing monochromatic waves.** We will now consider the case of a monochromatic wave for which the initial shape is prescribed but the wave profile as well as the orbital velocities can evolve dynamically under the action of the wind above the surface. The initial steepness is 0.1 The profile of the wave is given at any time t by $h(\mathscr{X},t) = a_0 - a_0\cos[k\mathscr{X}]e^{kc_it}$ Where c_i is the complex part of the phase speed, and a_0 is the initial amplitude.

The complex part of the phase speed c_i is calculated from the growth factor $\varsigma = kc_i$ through a model which couples air with water at the interface [19].

We express the inviscid equation for the amplitude, $\phi(\zeta)$, of mean perturbation velocity $U(\zeta)$ as

$$\Omega(\zeta) = (U-c)^{-1}[U'\phi - (U-c)\phi']^{-1}\phi$$

where Ω satisfies the Riccati equation

$$\Omega' = k^2(U-c)^2\Omega^2 - (U-c)^{-2} \tag{6.1}$$

According to Sajjadi *et al.* [20], the solution of (6.1) may be expressed as

$$w = U_0' c\left[\Omega_1 - \frac{1}{U_1'(U_1-c)} - \int_0^{\zeta_1} \frac{U''\,d\zeta}{U'^2(U-c)}\right][1+O(k\zeta_1)^2] \tag{6.2}$$

where the subscript 1 implies evaluation at the point $\zeta = \zeta_1$ defined such that

$$k|\zeta_c| < k\zeta_1 \ll 1, \qquad |U_1 - c| \gg c_i$$

Evaluation of the integral in (6.2), where the path of integration is taken under the sigularity at $\zeta = \zeta_c$, and taking the imaginary part, yields the approximation

$$w_i = \pi(U_0'/U_c')\gamma[1+O(k|\zeta_c|)^2], \qquad \gamma = -cU_c''/U_c'^2$$

The growth factor is then obtained from the secular equation [19] and may be expressed as

$$\varsigma = \frac{\rho_a}{2\rho_w}U_0'\left\{\frac{w_i - (\nu_a k/2c_r)^{\frac{1}{2}}[(U_c'/kc_r) + 2(w_r-1)]}{(w_r-1)^2 + w_i^2}\right\} \tag{6.3}$$

where ν_a and ρ_a are, respectively, the kinematic viscosity and the density of the air, ρ_w is the water density, U_0' is the gradient of U at the air-sea interface, the suffix c implies evaluation at the critical point $\zeta = \zeta_c$ and $w_r = 1 - c_r U_0' e^{-k\zeta_c}/U_c'^2$.

To reduce the computational costs the wave profile and the computational domain will only be updated every 75 iterations (limit for which the CLF condition is satisfied). All the variables will then be interpolated/extrapolated onto the new grid.

Figure (4) shows the streamlines at different time steps of the simulation. As the waves grows and become steeper the critical layer that is initially very close to the surface wave rises. The cat's eye pattern also grows in size and extend vertically what leads to an important disturbance of the mean flow.

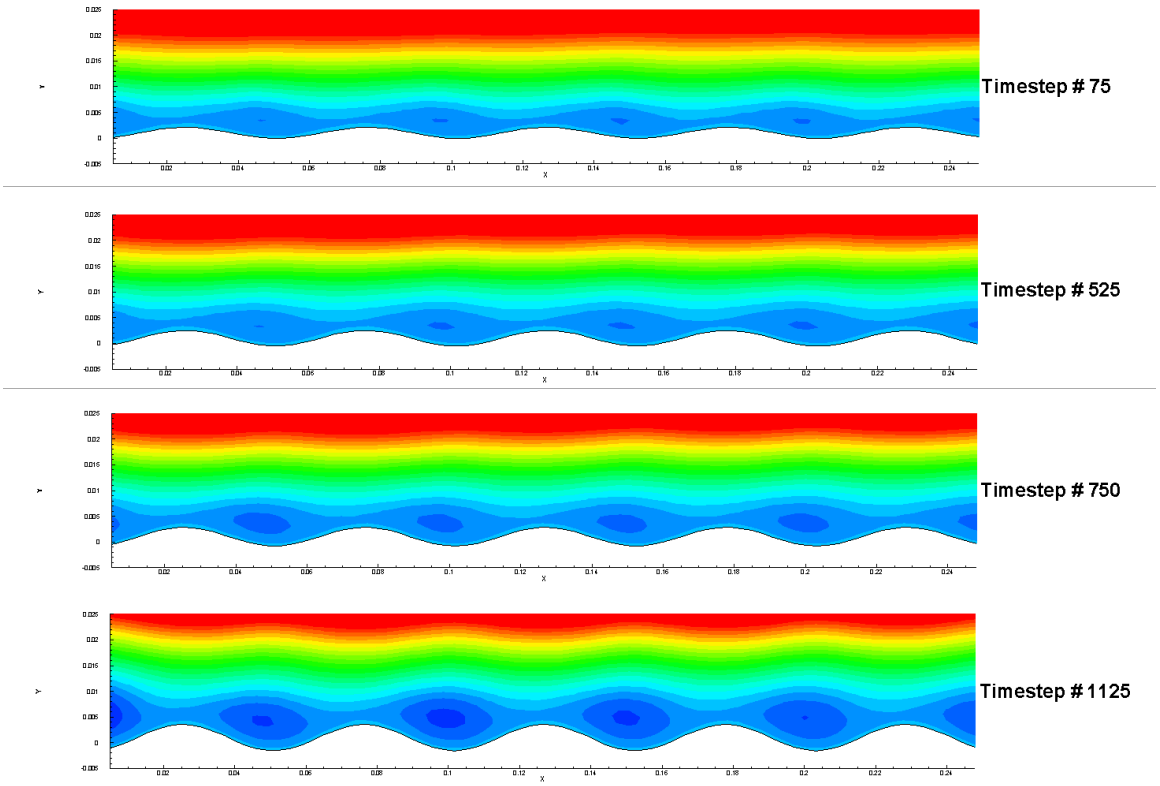

FIGURE 4. Streamlines for an alternate wave age of 0.47 and different steepnesses.

7. **Conclusions**

A coupled air-sea Reynolds stress model was successfully applied to non growing and growing monochromatic waves. The results obtained on the moving but non growing monochromatic waves is in accordance with the results found by Sullivan *et al.* [21] using direct numerical simulation. The height of the critical layer and the vertical extend of the cat's eye structures increase with the wave age and the steepness. As a monochromatic waves grows under the effect of wind, the height of the critical layer and the size cat eyes structures increase. Compared to a very computationally costly DNS simulation our model allow us to get a little closer to what happens in nature by working with an evolving mesh. But there remains much further investigations in order to model adequately the airflow over wind generated waves. There is no monochromatic wave in the ocean, waves travel in groups. Because of the asymmetry of the flow over a group of waves (waves growing on the upwind side of the group and decreasing on the downwind of the group), the critical layer height will spatially dependent over the waves of the group. These variations in the height of the critical layer will contribute to the energy input to the wave group. Thus the next step of our investigation will be an equivalent study on groups of waves.

REFERENCES

[1] M.A. Al-Zanaidi and W,H. Hui,Turbulent airflow over water waves-a numerical study *J. Fluid Mech.*, **148**, 225, 1984

[2] S.E. Belcher and J.C.R. Hunt, Turbulent flow over hills and waves, *Ann. Rev. Fluid Mech.*,30: 507–538,1998

[3] P. Cherukat, Y. Na, T.J. Hanratty and J.B. McLaughlin, Direct numerical simulation of a fully developed turbulent flow over a wavy wall, *Theor, Comput. Fluid Dyn.*, 11: 109–134, 1998. Polytechnic,

[4] V. De Angelis, P. Lombardi and S. Banerjee, Direct numerical simulation of turbulent flow over a wavy wall, *Phys. Fluids*,9:2429–2442, 1997

[5] O.A. Druzhinin, Y.I. Troitskaya and S.S Zilitinkevich, Direct numerical simlulation of a turbulent wind over a wavy water surface, *J. of Geophysical Research, Vol 117, Issue C11, 2012.*

[6] S. Fu, B.E. Launder and D.P. Tselepidakis, Accommodating the effects of high strain rates in modelling the pressure-strain correlation. *Rep. No. TFD/87/5*, Mechanical Engineering Department, UMIST, 1987.

[7] P.R. Gent and P.A. Taylor, Anumerical model of the air flow above water waves,*J. Fluid Mech.*, **77**, 105–128,1976.

[8] M. M. Gibson and B.E. Launder, Ground effects on pressure fluctuations in the atmospheric boundary layer, *J. Fluid Mech.*, **86**, 491, 1978.

[9] K. Hanjalic and B.E. Launder,A Reynolds stress model of turbulence and its application to thin shear flows. *J. Fluid Mech.*, **52**, 609, 1972

[10] B.P. Leonard,A stable and accurate convective modelling procedure based on quadratic upstream interpolation, *Comp. Maths. Appl. Mech. Eng.*, **19**, 59, 1979.

[11] M. J. Lighthill,The fundamental solution for small steady three-dimensional disturbances to a two-dimensional parallel shear flow *J. Fluid Mech.*, **3**, 113, 1957

[12] Mei-Ying Lin, Chin-Hoh Moeng. Wu-ting Tsai, P.P Sullivan and S.E. Belcher, Direct numerical simulation of wind wave generation processes, *J. Fluid Mech.*, Vol. 616, 1–30, 2008.

[13] C. Maas and U. Schumann,Numerical simulation of turbulent flow over a wavy boundary, *Proc. First ERCOFTAC Workshop on Direct and Large-Eddy Simualtions*,287–297, 1994

[14] C. Mastenbroek,Wind wave interaction Ph.d Thesis, *Delft Technical University*, 1996

[15] C. Mastenbroek, V.K. Makin, M.H. Garat and J.P. Giovanangeli, Experimental evidence of the rapid distortion of turbulence in air flow over waves, *J. Fluid Mech.*,**318**, 273, 1996

[16] J.W. Miles,On the generation of surface waves by shear flows,*J. Fluid Mech.*, **3**, 185., 1957

[17] S.V. Patankar, *N*umerical Heat Transfer and Fluid Flow, Taylor & Francis, 1980.

[18] S.G. Sajjadi, T.J. Craft, Y. Feng, A numerical study of turbulent flow over a two-dimensional hill. *Int. J. Numer. Meth. Fl.*, **35**, 1, 2001

[19] S.G. Sajjadi, J.C.R. Hunt and F. Drullion, Dynamics of critical layer in turbulent shear flows above unsteady water waves, to be submitted to *J. Fluid Mech.*, 2014

[20] S.G. Sajjadi, J.C.R. Hunt, F. Drullion, Asymptotic multi-layer analysis of wind over unsteady monochromatic surface waves. *J. Eng. Math.*, **84**, 73, 2013

[21] P.P. Sullivan, J.C. McWilliams and C.H. Moeng, Simulation of turbulent flow over idealized water waves *J. Fluid Mech.*, **404**, 47.2000.